Available online at www.sciencedirect.com
SCIENCE DIRECT
Geomorphology 78 (2006) 3–21
GEOMORPHOLOGY
www.elsevier.com/locate/geomorph

Fluvial response to large rock-slope failures: Examples from the Himalayas, the Tien Shan, and the Southern Alps in New Zealand

Oliver Korup [a,*], Alexander L. Strom [b], Johannes T. Weidinger [c]

[a] WSL Swiss Federal Institute for Snow and Avalanche Research SLF, CH-7260 Davos, Switzerland
[b] Institute of Geospheres Dynamics, Russian Academy of Sciences, Moscow, Russia
[c] Department of Geography, Geology and Mineralogy, University of Salzburg; Erkudok© Institute, Kammerhofgasse 8, A-4810 Gmunden, Austria

Received 22 April 2005; received in revised form 29 September 2005; accepted 13 January 2006
Available online 23 February 2006

Abstract

We describe remnants of large (10^7–10^{10} m^3) Late Pleistocene to Holocene rockslides and rock avalanches that block(ed) rivers and are preserved in the Himalayas, the Tien Shan, and the New Zealand Southern Alps despite rates of uplift and erosion of up to 10 mm $year^{-1}$. These natural dams control fluvial response on 10^1–10^4 year timescales by (a) storing and releasing sediment during forced alluviation and fluvial re-incision; (b) relocating river channels through diversion or seepage; (c) inhibiting river erosion into bedrock; (d) forming persistent long-profile knickpoints and knickslopes associated with steep high-energy ($>10^3$ W m^{-2}) breach and epigenetic bypass gorges and fluvial hanging valleys; and (e) shaping valley-floor morphology. Sediments indicate that rockslide-dammed lakes may persist up to 10^4 years, before being drained or infilled. Several short-lived (10^0–10^2 year) historical rockslide dams in the Indian and Nepal Himalayas and the Southern Alps have had marked volumetric impacts on catchment sediment budgets shortly following failure. Therefore, we caution against the linear extrapolation of sediment delivery from prehistoric rockslide dams through time as a response variable. We find reach-scale changes to channel gradient to be prominent and persistent indicators of fluvial response to large rock-slope failures.

Keywords: Landslide dam; Fluvial response; River long profile; Sediment yield; Mountain geomorphology

1. Introduction

Landslide dams are a common type of river disturbance in tectonically active mountain belts (Costa and Schuster, 1988; Pushkarenko and Nikitin, 1988; Clague and Evans, 1994; Chai et al., 2000; Hewitt, 2002; Korup, 2004a). They are often portrayed as ephemeral features, given that ~80% of historically documented cases that failed, did so within 1 year (Ermini and Casagli, 2003). The potential of many landslide dams to generate catastrophic outburst flows has focused research attention largely on stability criteria and immediate hydrogeomorphic impacts because of sudden dam failure.

Little work exists on the long-term geomorphic history of rivers following the failure of natural dams, although input of excessive sediment from large catastrophic rock-slope failures may cause significant channel instability (Korup, 2004b; Korup et al., 2004). Fluvial response to such pulsed supply of hillslope sediment may theoretically involve adjustment of sediment yield, channel planform, cross-section,

* Corresponding author. Tel.: +41 81 417 0354.
E-mail address: korup@slf.ch (O. Korup).

0169-555X/$ - see front matter © 2006 Elsevier B.V. All rights reserved.
doi:10.1016/j.geomorph.2006.01.020

gradient, or bed configuration. Among these potential response variables, configuration of the channel bed, cross-section, planform, and gradient require increasingly higher adjustment times, ranging from 10^{-1} to 10^{3} years (Knighton, 1998).

Our interest here is investigating long-term fluvial response, hence we focus on channel gradient as a potential indicator. The hypothesis is that formation of a sufficiently high rockslide dam would cause a fluvial response marked enough to be recognised in the river long profile. We use the height of the rockslide dam and channel steepness as measures to quantitatively test this hypothesis. Prehistoric rockslide dams should offer insights into such fluvial response over a range of timescales, through characteristic assemblages of hillslope, fluvial, and lacustrine landforms and sediments (Hewitt, 2002).

Therefore, we augment this quantitative analysis with field observations of rivers dammed by large ($>10^{6}$ m^{3}) catastrophic rockslides and rock avalanches (terminology follows Cruden and Varnes, 1996). To stress the ubiquity of this phenomenon, we selected the Himalayas, the Tien Shan, and the Southern Alps in New Zealand, as prime examples of tectonically active mountain belts with high rates of uplift and erosion, and frequent slope failure (Table 1).

2. Study areas

2.1. Himalayas

The Himalayas are the product of continent–continent collision between the Indian and Eurasian Plates, since 65 Ma along the Indus-Zangbo-Suture Zone. The parautochthonous sedimentary sequence of the Tibetan Himalayas (Proterozoic–Eocene) partly forms the summit areas of the highest peaks on Earth (Mt. Everest, 8848 m a.s.l.), and is locally detached from the High Himalayan Crystalline (HHC) by the South Tibetan Detachment Zone.

Further south, crustal thrust planes formed within the Indian Plate at 25–20 Ma. The Main Central Thrust (MCT) is a km-scale mylonitic zone, which detached gneisses, migmatites and granites of the HHC from Precambrian metasediments and crystalline nappes of the Lesser Himalayas. The Main Boundary Thrust (MBT) divides the nappe systems of the Lesser Himalayas from the Sub-Himalayas (Miocene–

Table 1
Key characteristics of the Himalayas, Tien Shan, and the Southern Alps in New Zealand

	Himalayas	Tien Shan	New Zealand Southern Alps
Location	India, Nepal, Bhutan	Kazakhstan, Uzbekistan, Kyrgyzstan, Tajikistan, China	South Island, New Zealand
Dimensions	2500 km × 200–250 km	1500 km × 200–300 km	~800 km × 200 km
Morphotectonic setting	Continent–continent collision (Eurasian and Indian Plates) along Indus-Zangbo-Suture Zone	Intraplate compressional zone caused by India–Eurasia collision	Dextral transpressional continent–continent collision (Australian and Pacific Plates)
Seismicity	Increasing from N to S (displacement on MCT shifted mainly to MFT), $M<8.6$ earthquakes every 30 years	M 7–8 earthquakes at N and S fringes every 40–50 years; presently less active in interior	Historically shallow; $M\sim8$ earthquakes every 250–300 years on Alpine Fault
Lithology at study sites	Sedimentary (Tibetan zone); metamorphic crystallines (Lesser and Higher Himalayas)	Palaeozoic to Cenozoic terrigeneous and carbonate sedimentary, metamorphic, and igneous rocks	Greywacke with various metamorphic overprints (up to greenschist/oligoclase facies)
Crustal shortening (mm year^{-1})	1–20	10–12	36–38
Uplift (mm year^{-1})	1–15	1–2	1–10
Total relief (km)	~8	~7	~4
Climate	Highly seasonal (SW summer monsoon); subtropical in the S; humid to arid from E to W	Continental arid to semi-arid	Perhumid mild oceanic to moderately continental
Precipitation (mm year^{-1})	6000 in E; 1500 in central parts (Nepal); 250–500 in W	200–400 (intermontane basins); 800–1000 (mountain ranges)	800–15000
Glacier extent	Generally high; snowline ≥4400 m a.s.l. in SE, and 5100–5800 m a.s.l. in NW	2% presently covered by ice; snowline from 3600–4450 m a.s.l. (NW and central)	11% presently covered by ice
Mean denudation (mm year^{-1})	<12	unknown	<10
Sediment yield (t km^{-2} year^{-1})	10^{2}–10^{4}	10^{2}–10^{3}	10^{2}–10^{4}

Pleistocene), mainly composed of the molasse-type Siwalik Formation (Upreti, 1999). Crustal shortening of 20 mm year^{-1} is largely accommodated by the Main Frontal Thrust (MFT), and uplift ranges between 1 and 15 mm year^{-1} in the Higher Himalayas and the Siwalik Hills, respectively (Lavé and Avouac, 2001; Table 1).

High rates of uplift and extremely seasonal precipitation favour intensive erosion and mass wasting. Location and orientation of rock-slope failures are mainly pre-designed by tectonics and sliding planes parallel to foliation and rock strata (Schramm et al., 1998; Weidinger et al., 2002). Giant rock flow (Cruden and Varnes, 1996) with deep pre-existing joints and fissures has shaped many postglacial mountain flanks.

2.2. Tien Shan

The Tien Shan is an intraplate mountain belt that formed between the Tarim Basin and the Kazakh Shield because of the India-Eurasian collision (Molnar and Tapponier, 1975). Several Palaeozoic orogenies formed a complex basement structure, and a pre-Oligocene peneplain serves as an excellent marker for neotectonic deformation (Makarov, 1977; Chedia, 1986). Modern orogeny of the Tien Shan started in the Oligocene (Chedia, 1986) through complex basement folds divided by numerous reverse faults with significant lateral offsets (Delvaux et al., 2001). The mountain belt is crossed by several regional fault zones, e.g. the Nikolaev's Line and the Talaso–Fergana fault, separating the North Caledonian from the South Variscian zone, and the western and central Tien Shan, respectively.

The dissected relief of the Tien Shan is characterised by mainly W–E trending ranges several tens of kilometres long, 5–20 km wide, and 4.5–5.5 km high. Southeast of Lake Issyk-Kul, the Victory and the Khan-Tengri Peaks rise to >7000 m a.s.l. (Table 1). Topographic ridges and most major valleys correspond to neotectonic anticlines and intermontane tectonic depressions, respectively, linked by narrow transverse gorges, and composed of Neogene and Quaternary sand- and siltstones with gypsum beds, and conglomerates.

GPS data indicate mean transverse compression of 10–12 mm year^{-1} (Abdrakhmatov et al., 1996), resulting in high seismicity. Most of the $M>8$ historic earthquakes occurred at the southern and northern fringes of the mountain belt. The spatial pattern of recent faults and large rockslides indicates that the central Tien Shan may be as seismically active as its border zones.

2.3. Southern Alps in New Zealand

The Southern Alps in New Zealand result from oblique continental collision of the Australian and Pacific Plates along the 600-km long Alpine Fault. Dextral transpression has exhumed partially metamorphic Triassic greywacke from depths of >20 km since 5 Ma (Norris and Cooper, 2000). The Southern Alps rise to nearly 3800 m a.s.l. and are deeply dissected. Major backthrust occurs along the main divide, and numerous oblique reverse, normal, and strike-slip faults pre-designed the course of major alpine valleys (Long et al., 2003). Metamorphic overprint of greywacke increases up to amphibolite schist grade at the Alpine Fault, whereas subgreenschist and unaltered greywacke/argillite facies dominate E of the divide. Several deformed terranes also featuring ultramafic rocks were accreted to the SW fringe of the Southern Alps (Norris and Cooper, 2000). Uplift and erosion rates are <11 mm year^{-1} near the Alpine Fault, and ~1 mm year^{-1} E of the divide (Tippett and Kamp, 1995; Table 1).

The mountain belt intercepts moisture-bearing winds from the Tasman Sea, and receives precipitation of up to 14 m year^{-1} W of the divide (Henderson and Thompson, 1999). Repeated Quaternary glaciations deposited large moraines at the mountain fringe. Whitehouse (1988) subdivided the Southern Alps into a Western (WSA), Axial (ASA), and Eastern (ESA) part. Valleys in the WSA are generally steep, V-shaped, closely spaced, and rejuvenated by coseismic changes in base level. The ASA have the highest elevations and are dominated by glacial landforms. In the ESA, basins are larger and characterised by moraine-fringed valley trains and ice-scoured lake basins.

Causes of rock-slope instability in the Southern Alps are gravitational stress, lowering of rock-mass strength through earthquake shaking, hanging-wall shattering, and incision-driven loss of lateral support. Trigger mechanisms include earthquakes, high-intensity rainstorms, and fluvial undercutting (Korup, 2005). Several historic rock avalanches occurred without any observed triggers, possibly from exceeded intrinsic stress thresholds, and catastrophic culmination of rock flow (McSaveney, 2002).

3. Methods

The large number of documented rockslide dams in these study areas is compromised by incomplete or low-resolution geomorphometric data. Therefore, we used topographic maps, air photos, satellite images, and digital elevation models (DEMs) at 25-m (Southern

Alps), ~80-m, and ~860-m (Tien Shan, Himalayas; 3″ SRTM and USGS GTOPO30) grid resolution to extract river long profiles and measure rockslide, catchment, and channel geometry. Volumes of reservoir infill and debris removed by fluvial incision were estimated from extrapolating contour lines across preserved terraces and erosional scarps, respectively. Fieldwork included ground truthing and geomorphic mapping of key landforms and sediment bodies related to rockslide dams.

In the Indian and Nepal Himalayas, 24 of the numerous large rockslide and rock-avalanche dams were studied in detail (Weidinger, in press). The Tien Shan hosts >100 former rockslide dams identified to date, with some 20 lakes presently impounded. In the Southern Alps, >40 rockslide/avalanche dams are known, of which <10% presently retain lakes. Our selection of examples draws from an ongoing data compilation of rockslide dams in active mountain belts (Strom, 1998; Korup, 2004a; Weidinger, in press).

We focus on sites where age and size of the rockslide, and fluvial response, are reliably constrained by geomorphic evidence, and the height of the dam is large enough to be identified at the available DEM resolution. To encompass a broad range of timescales, we compare Pleistocene/Holocene with historic cases, combining field interpretations with geomorphometric analyses to highlight key processes involved. We do not claim that these examples contain or explain the full range of possible response of mountain rivers to large rock-slope failures. Instead, we use selected case studies to address varying response times, and similarities in fluvial response despite differing tectonic and climatic boundary conditions.

We quantitatively analysed river long profiles to detect the geomorphic imprints of large rockslide dams on channel gradient. The relative steepness of channel reaches can be objectively quantified via the empirical relationship

$$S = k_s A_C^{-\theta}, \quad (1)$$

where S=channel slope, A_C is upstream catchment area, k_s is the steepness index [$m^{2\theta}$], and θ is the concavity index (e.g. Whipple and Tucker, 1999). Using linear reduced major axis regression of log$S$ and logA_C for an arbitrarily fixed θ allows mapping of along-profile variation in k_s (Hodges et al., 2004). We used θ=0.45 (a typical value for rivers in active mountain belts) to test whether breach channels would be exceptionally steep compared to the remaining profile.

To characterise fluvial process response, we collected long-term rates of fluvial incision, and also estimated specific stream power

$$\Omega = Q\rho S w^{-1}, \quad (2)$$

where Q is discharge, ρ is water density, g is gravitational acceleration, and w is active channel width, which we measured from 2-m resolution orthophotos.

4. Fluvial response to rock-slope failures

4.1. Giant prehistoric failures

Historically, dams from rock-slope failure were often breached rapidly (Ermini and Casagli, 2003). Yet, examples from the Himalayas and the Tien Shan show that long-term blockage may occur, affecting even large ($A_C > 10^4$ km^2) mountain catchments (Table 2).

4.1.1. Kalopani rockslide, Kali Gandaki River, Nepal

The Kali Gandaki River drains the Thakkhola graben across the High Himalayas in an impressive gorge, along which numerous lake-damming rock avalanches have impacted the morphology of the valley-floor (Fort, 2000). The largest (~3×10^9 m^3) is the breached Kalopani rockslide dam (Hormann, 1974; Fort, 2000; Fig. 1), which caused deposition of 1.5–3×10^9 m^3 of Late Pleistocene to Holocene alluvial, lacustrine, and mass-wasting sediments over 30 km upstream. Among these, the 200-m thick lacustrine Marpha Formation was interpreted to be associated with a major landslide dam between 79±11 and 29±4 ky (Fort, 2000). Although this may have been the Kalopani rockslide, it is also possible that episodic ice-mud-debris-avalanches from nearby Nilgiri (7061 m a.s.l.) contributed to multiple river blockage (Weidinger, in press). The lake(s) must have been emptied by the Mid-Holocene, because Saijo and Tanaka (2002) noted soil development below the level of lake sediments commencing at ~5 ky BP.

4.1.2. Beshkiol, Naryn River

Another giant (~10 km^3) rockslide is located near Beshkiol, Naryn River, Tien Shan. Failure of a part of the Akshiyriak Range affected ~60 km^2 (Strom, 1998), and infilled the valley with debris over ~7 km to slightly above the level of a tectonic bench (Fig. 2A,B). We interpret a nearly horizontal terrace at ~1640 m a.s.l., which extends ~70 km upstream, as a former lake level. The lake had an inferred volume of 15–20 km^3,

Table 2
Characteristics of large rockslides and rock avalanches that block(ed) rivers

Region Name	River	Age	Geology	V_L (10^6 m^3)	H_D (m)	W_D (km)	L_D (km)	L_{ch} (km) (% of total basin length)	A_C (km)^2	H_C (km) (% of total basin relief)	S
Himalayas											
Kalopani	Kali Gandaki	79±11 to 29±4 kyr	Augen/biotite gneiss	3000	400–900	6	4	30 (5%)	51500	4.4 (20%)	0.08
Dukur Pokhari	Marsyandi	Holocene	Limestone, schist	1000	100–300	2.3	1	5 (3%)	634	4.1 (2%)	0.079
Latamrang	Marsyandi	5400BP	Gneiss, quartzite	4500[a]–5500	300–700 80–100	4	2.5	>9 (>5%)	1763	5.1 (14%)	0.073
Tal	Marsyandi	<1000 BP	Sillimanite gneiss	4.5		1	0.5	3.8 (2%)	2373	5.8 (2%)	0.068
Gohna Tal	Birahi Ganga	AD1893	Dolomites, limestone, marls, schists	150–200	275, 120[b]	1.6	0.8	5 (12%)	253	4.1(6%)	n.d.
Jagat	Buri Gandaki	AD1962–1979	Pulverized, cataclastic rocks	200	90–100	1.5	1.5	8 (5%)	3117	6.0 (3%)	0.095
Labubesi	Buri Gandaki	1968	Pulverized, cataclastic rocks	200	100	1.5	1.5	8 (5%)	3740	6.6 (3%)	0.097
Tien Shan											
Beshkiol	Naryn	?Holocene	Neogene sandstone, conglomerate, gypsum	8000–12000	300–350	7	~1.5	70 (17%)	34000	3.4 (9%)	0.013
Djashilkul	Chon-Kemin	?Holocene	Palaeozoic metasediments	400–500	150–200	2	1.1	>2.3 (>2%)	1100	2.7 (4%)	0.03
Aksu	Aksu	Holocene[c]	Palaeozoic granite, meta-sediments	1500	200–450	2.5	2	4 (10%)	320	2.6 (9%)	0.091
Southern Alps (NZ)											
Falling Mountain	Otehake	AD1929	Mesozoic greywacke, argillite	55	80[d] 80	–	–	4.5 (100%)	8.6	1.2 (100%)	0.124
Mt Adams	Poerua	AD1999	Schist, colluvium	10–15		0.6	0.5	>6 (37%)	50	2.3 (8%)	
Zig-Zag	Otira	2000BP	Mesozoic greywacke, argillite	43	100	1.0	n.d.	>1.8 (>6%)	15	1.6 (12%)	0.166
Polnoon Burn	Shotover	4000BP	Schist	140	110	1.5	1.2	>3.8 (11%)	32	1.2 (11%)	0.11

V_L=rockslide volume; H_D, L_D, W_D=rockslide dam height, length, and width, respectively; L_{ch}=total affected channel length; A_C, H_C=upstream catchment area and relief, respectively; S=channel slope.
[a] Remnant volume.
[b] H_D after first outburst.
[c] Subsequent failure during 1885 earthquake.
[d] Inferred maximum thickness of valley infill, minor tributary damming only.

and a mean depth of 70 m. Overflow of the lake formed a sinuous, 10-km long and 300-m deep, bypass gorge cut through hard Palaeozoic rocks around the rockslide toe. Oversteepened convex profiles at tributary mouths north of the gorge indicate delayed fluvial response to rapid bedrock incision (1–3, Fig. 2C). Although we cannot fully exclude additional tectonic uplift, these fluvial hanging valleys are at odds with tributary profiles further upstream of a more regular profile shape (4–5, Fig. 2C), which we interpret to reflect adjustment to gradual aggradation behind the dam. Seepage may have also occurred through the Neogene debris intercalated

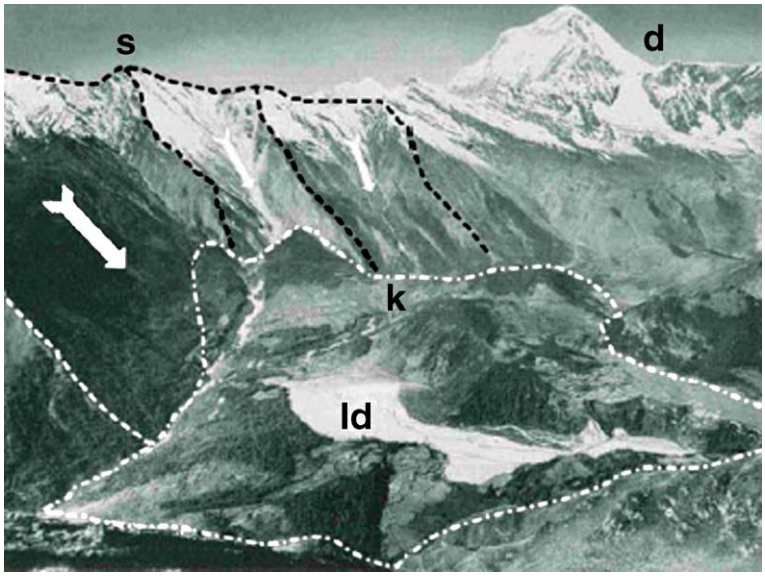

Fig. 1. SE–NW view from Nimek Peak (3900 m a.s.l.) across Kali Gandaki River towards rockslide dam (ld, ~3×10^9 m^3) near Kalopani (k), partly infilled by alluvial gravel; d=Dhaulagiri (8172 m a.s.l.), s=Sarpang Dhuri (scarp), →=direction of movement. Image based on original photo by Hormann (1974).

with solution-prone gypsum beds. At the present-day mean yield of suspended sediment $Q_s=4\times10^6$ m^3 $year^{-1}$ (+20% for bed load; A. Zhirkevitch, personal communication, 2005), silting up of the lake would have roughly taken 3000–4000 years at an estimated rate of 5×10^6 m^3 $year^{-1}$.

4.2. Multiple rockslide dams and reactivations

The long-term blockage of large mountain rivers by such single giant failures provides ideal conditions to track fluvial response to a single disturbance. Very often, however, several rockslides occur along the length of a river, including reactivation at a given site.

4.2.1. Marsyandi River, Nepal

The Marsyandi River drains the Annapurna and Manaslu massifs of Central Nepal and, like the Kali Gandaki, shows evidence of multiple large (>10^8 m^3) rock-slope failures (Weidinger, in press). For instance, Late Pleistocene and postglacial advances overrode debris of the 5-km^3 Braga rockslide, which had infilled the upper valley to a height of 200 m, now completely dissected to a remaining mass of 1–2 km^3 (Fig. 3). Between the upper and lower Marsyandi valley, the composite rockslide of Dukur Pokhari had formed a 1-km^3 dam, which has remained largely intact (Figs. 4A and 5A).

Another giant rockslide at Latamrang buried ~4 km of the valley floor, and dammed the river to form a long and narrow lake (Weidinger and Ibetsberger, 2000; Fig. 4B,C). Swash debris is preserved up to 500 m above the present channel. Remnants of lacustrine sediments on the flanks of the former reservoir yield ages of 5.4 ky, whereas infilling of the lake and dissection of the dam and the impounded sediments must have occurred within ~500 years (B. Pratt-Sitaula, personal communication, 2005).

Finally, a yet smaller rock avalanche dammed the valley at Tal, 7 km South of the Dudh Khola confluence <1000 years ago (Weidinger and Ibetsberger, 2000; Fig. 5A). The original lake volume of $10–15\times10^6$ m^3 was filled with alluvium within <200 years and a boulder-armoured spillway gorge has subsequently cut around the distal and largely intact dam deposit (Fig. 4D,E). Further downstream, a 70–120 m high terrace is interpreted as the deposit of a 4-ky-old landslide/debris-flow from Ngadi Khola that infilled the valley with ~1.5 km^3 of debris over a length of 40 km (Pratt-Sitaula et al., 2004).

4.2.2. Aksu River

Reactivation of blockage at the same site is illustrated by the ~1.5-km^3 Aksu rockslide in the northern Kyrgyz Range, Tien Shan. There, Palaeozoic granites and metasediments fell over 1800 m from the right valley wall, forming a dam >400 m high.

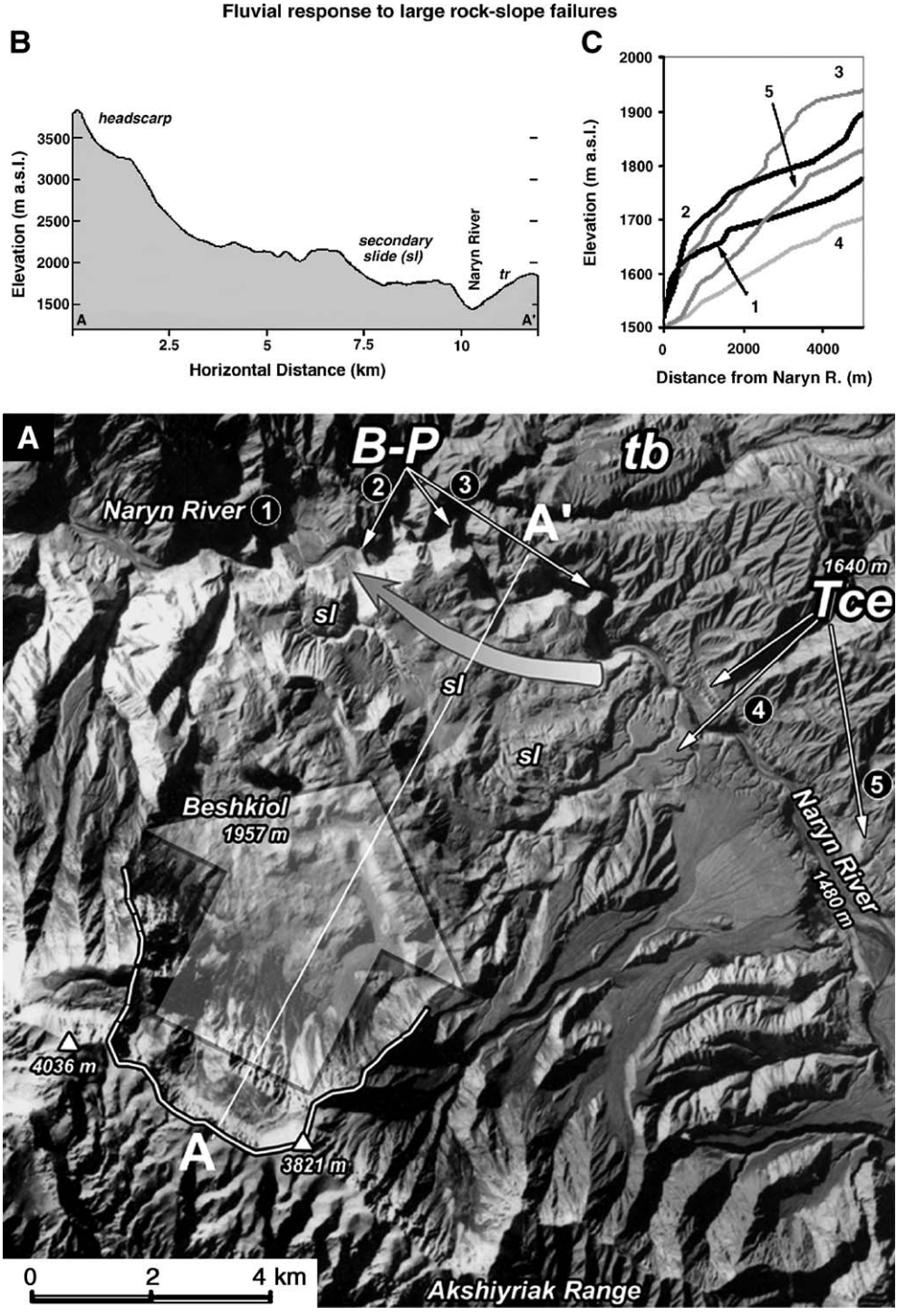

Fig. 2. (A) KFA-1000 satellite subscene (FN 1051/Frame 21626) of the giant (10^{10} m^3) Beshkiol rockslide dam on Naryn River, Kyrgz Tien Shan, forming a 70-km long lake (inferred from lake terraces, Tce). Curved →=inferred former river course. Fluvial response involved cutting of a 10-km long and 300-m deep bypass gorge (B–P) into hard Palaeozoic rocks of a tectonic bench (tb); sl=secondary landslides; 1–5=tributaries (see C). (B) Long profile of rockslide. (C) Contrast in tributary long profiles showing fluvial hanging valleys because of delayed response to rapid gorge incision (1–3), and more adjusted tributaries (4–5) responding to gradual backwater aggradation.

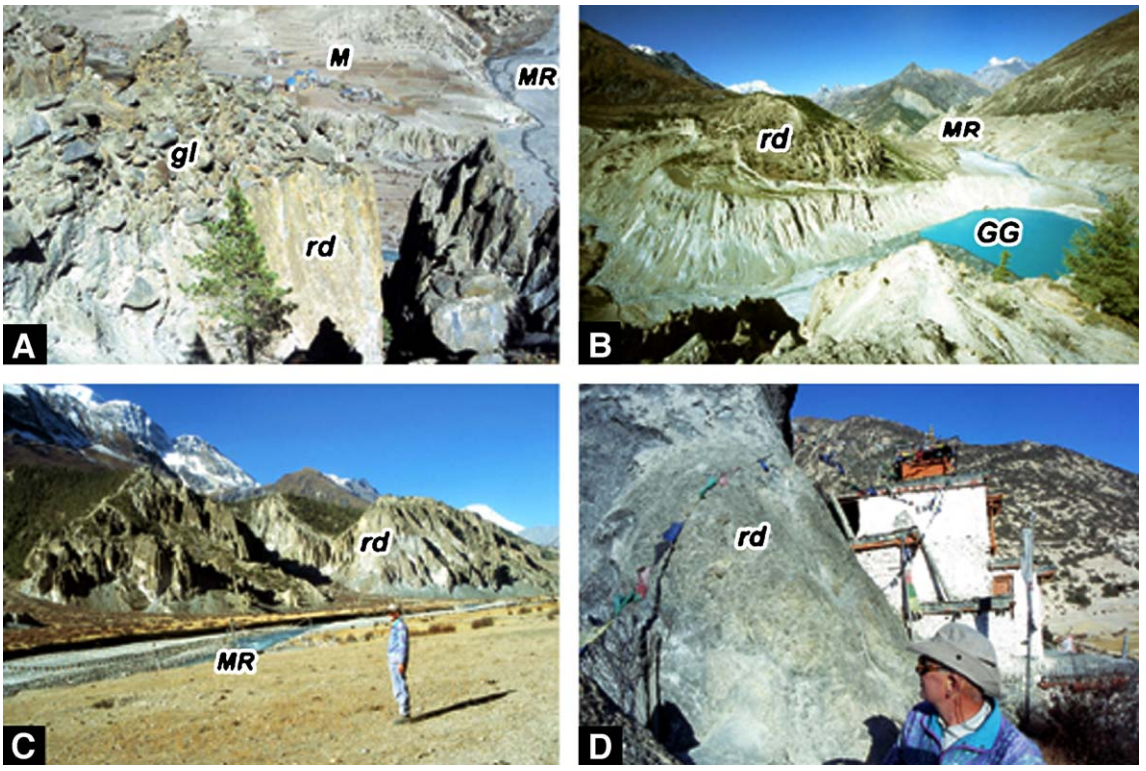

Fig. 3. Braga rockslide, upper Marsyandi River (MR), Nepal Himalaya: (A) View from "Glacier View Point" (3800 m a.s.l.): rockslide debris (rd) covered by terraced glacio-fluvial sediments (gl); Manang village (M) in the background, ~200 below. (B) View NW across the Gangapurna glacier lake (GG, 3780 m a.s.l.): lateral and terminal moraines of Gangapurna glacier (which reached Manang ~100 years ago) cover the rockslide debris. (C) Terraced and dissected debris. (D) Outcrop of dissected rockslide debris near the monastery of Braga (3450 m a.s.l.), showing cataclastic and re-cemented fragments.

Bedrock outcrops with rounded alluvial boulder lag up- and downstream of the blockage delineate a pre-failure course of the Aksu River several hundreds metres W from its present position. The absence of lake deposits indicates rapid breaching of the dam. Assuming a present-day discharge ($Q \sim 150 \times 10^6$ m^3 year^{-1}) to produce the former lake volume $V_{\mathrm{Lake}} \sim 50\text{–}100 \times 10^6$ m^3, the dam would have been overtopped in less than 1 year and formed a 200-m deep headward eroding breach channel (Fig. 5B). This breach channel was blocked at least once more by failure of undercut rockslide debris, possibly during the 1885 Belovodsk earthquake (Ignatiev, 1886). Part of the dam still exists, and the Aksu River upstream meanders through the infilled small lake depression (Fig. 5B).

4.3. Persistent geomorphic impact from Holocene rockslide dams

Not all of the rockslides of confirmed or inferred Holocene age in our study areas have retained long-lived lakes; several dozens of large dams are incised by steep breach gorges.

4.3.1. Djashilkul, Chon-Kemin River

In the Tien Shan, the 200-m high Djashilkul rockslide is one out of a cluster of four large prehistoric failures, which had dammed the Chon-Kemin River and its tributaries (Strom and Abdrakhmatov, 2004). The lake was 5–7 km long and contained $\sim 200 \times 10^6$ m^3 of water. Using present-day values of discharge, overtopping may have occurred within a few months, confirmed by very thin lacustrine layers onlapping alluvial gravel. Dam breach was rapid and, most likely, catastrophic, indicated by a 40-m high terrace, composed of angular bouldery debris of the same lithology as that of the landslide deposit, immediately downstream from the breach channel (Fig. 6A,B).

4.3.2. ZigZag rock avalanche and Polnoon Burn rockslide, Southern Alps

Two further examples of Late Holocene rock-slope failures in the Southern Alps highlight the persistent

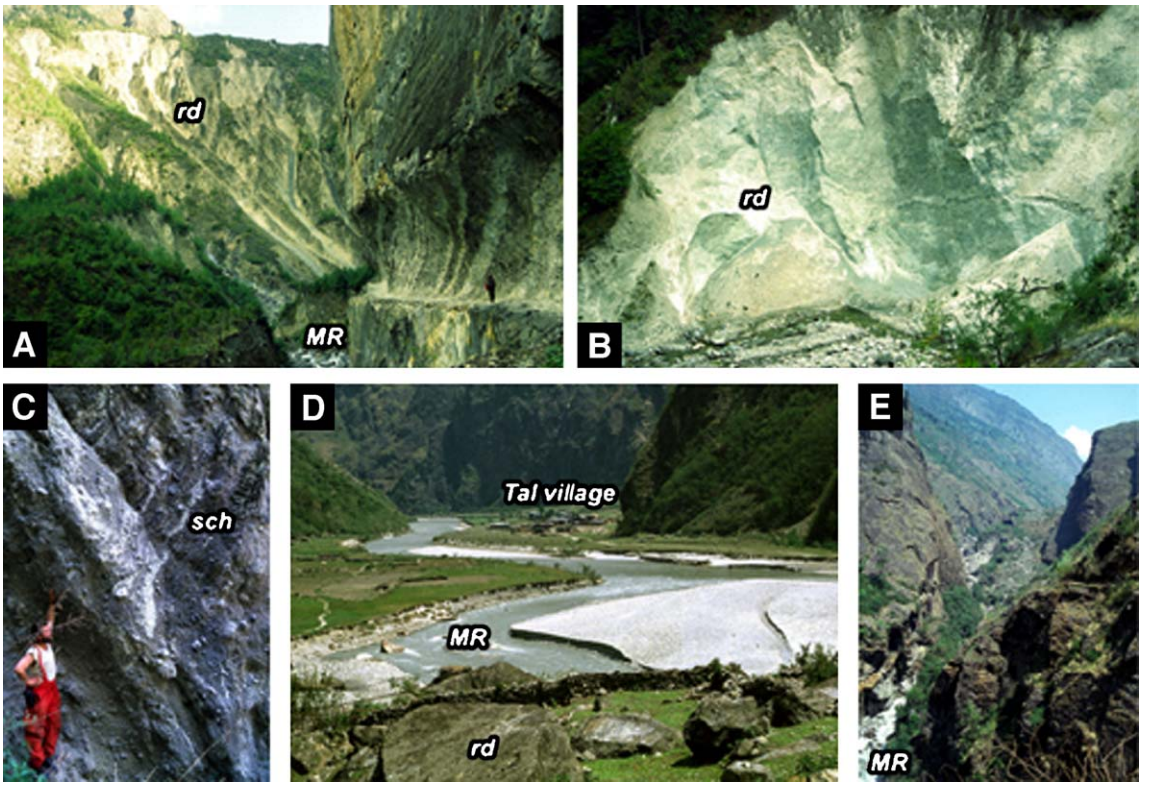

Fig. 4. (A) Upstream view of the shattered rockslide debris (rd) of Dukur Pokhari, Marsyandi River (MR), Nepal Himalaya, which is highly susceptible to erosion; 0.6 km W of Bhratang (3000 m a.s.l.). (B) Pulverized quartzite (several tens of m thick) at the base of Latamrang rockslide due to mechanical stress during sliding; 3 km W of Latamrang (2500 m a.s.l.). (C) "Schlieren" (sch) of diamicton in Latamrang slide debris on left bank of MR, 0.6 km East of Latamrang (2610 m a.s.l.). (D) Upstream view to infilled backwaters of Tal rock avalanche (1650 m a.s.l.). (E) Upstream view of bypass gorge around largely intact Tal rock-avalanche dam (2.5 km South of Tal, 1550 m a.s.l.).

effects of breach channels on the river long profile. The ZigZag rock avalanche, Otira River, and the Polnoon Burn rockslide (Fig. 6C), which retained a lake for ~2000 years, formed prominent headward-eroding knickslopes (Fig. 5C,D; Whipple and Tucker, 1999). Convex knickpoints mark the transition of low-gradient alluviated backwater reaches to steep breach gorges.

4.4. Historic examples

Several historic examples of rockslide dams in our study areas can be used to infer average rates of fluvial processes. Reservoir volume and upstream catchment area, A_C, allow rough estimates of rates of lake infilling by fluvial and hillslope sediment. Similarly, the amount of debris eroded from the dam divided by the time since breaching crudely indicates minimum sediment discharge and yield following failure, which in the WSA may attain 10^4 m^3 km^{-2} $year^{-1}$ (Table 3).

4.4.1. Gohna Tal rockslide, Garhwal Himalaya, India

The 1893 Gohna Tal rockslide dam on the Birahi Ganga, a tributary of the Alakananda River (Weidinger, 1998), exemplifies the sediment retention capability of historic events. Although overtopping and catastrophic failure occurred in 1894, forming four terraces on the flanks and downstream of the eroded dam (Fig. 7), the lake did not empty completely. The remnant lake took 78 years to infill despite an inferred upstream yield of sediment of >4000 m^3 km^{-2} $year^{-1}$ (Table 3). Although the river fully incised the dam, it has not yet cut down through the alluvial sediments and still meanders on top of them before it enters the breach channel.

4.4.2. Buri Gandaki River, Lesser Himalayas, Nepal

High rates of infill were estimated for the rockslide dams of Jagat (formed between 1962 and 1979) and Labubesi (1968) on the Buri Gandaki River, Manaslu-Kutsang-Ganesh Himal, Nepal. Both formed

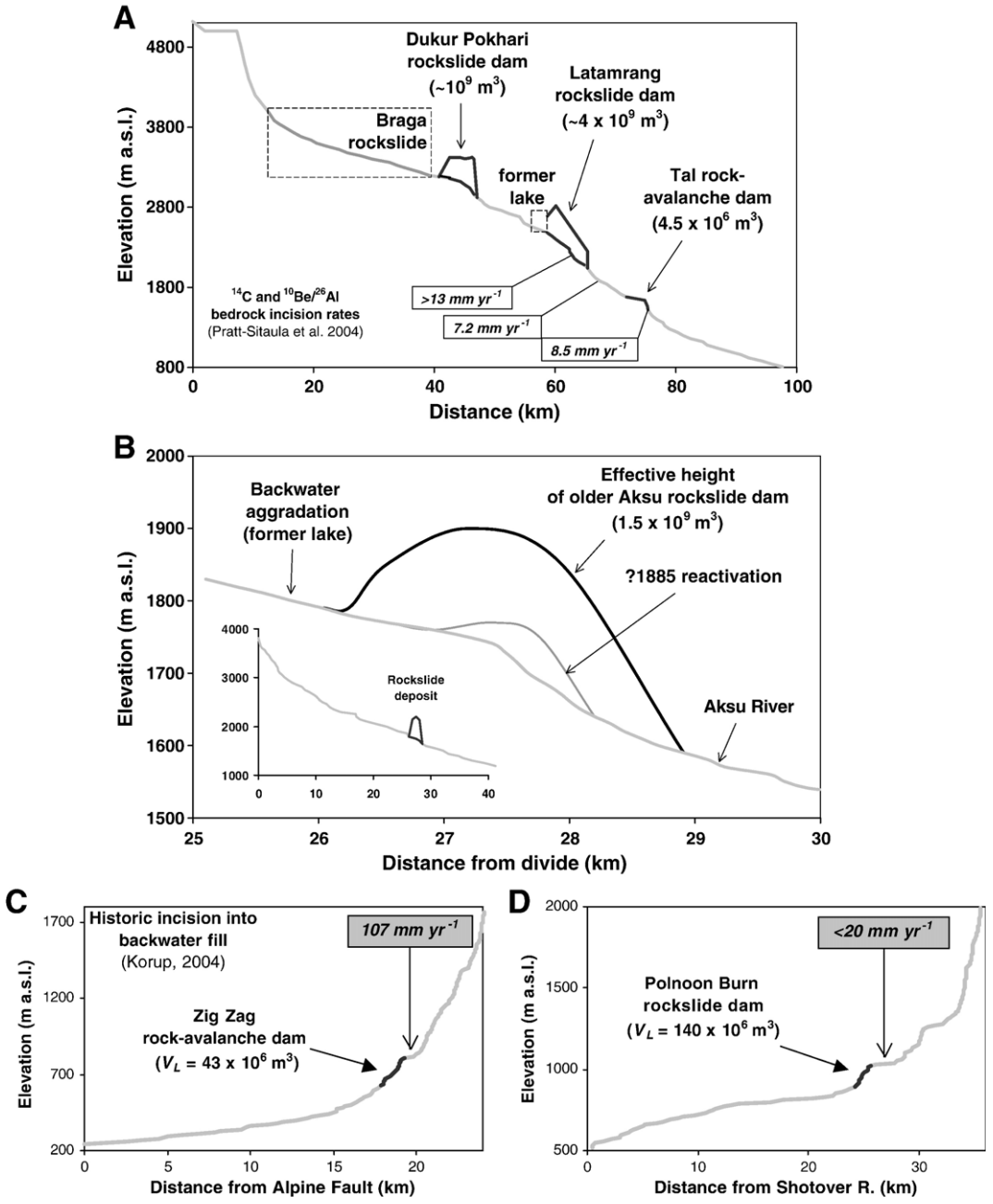

Fig. 5. Long profiles of rivers formerly blocked by large rock-slope failures. (A) Marsyandi River, Nepal Himalaya. (B) Aksu River, Kyrgyz Tien Shan. (C) Otira River, WSA, New Zealand. (D) Polnoon Burn, ESA, New Zealand. Note formation of knickslopes (A–C) and contrast between high rates of fluvial incision and preservation of Mid-to Late Holocene rockslide deposits.

ephemeral lakes, which were infilled within <17 years, at average yield rates of $>1.6\times10^4$ t d^{-1} (Jacobsen, 1990; Table 3). Although the dams were subsequently dissected, both dam-breach channels have not yet fully cut through the aggraded material, thus forming 50-m high prominent steps in the long profile.

4.4.3. Downstream impacts and river metamorphosis

Two historic examples in the western Southern Alps (WSA) illustrate catastrophic deposition and rapid infilling of bedrock channels by rock avalanches. During the 1929 M_S 6.9 Arthur's Pass earthquake, the summit of Falling Mountain (1901 m a.s.l.) fell as a rock avalanche onto the main divide

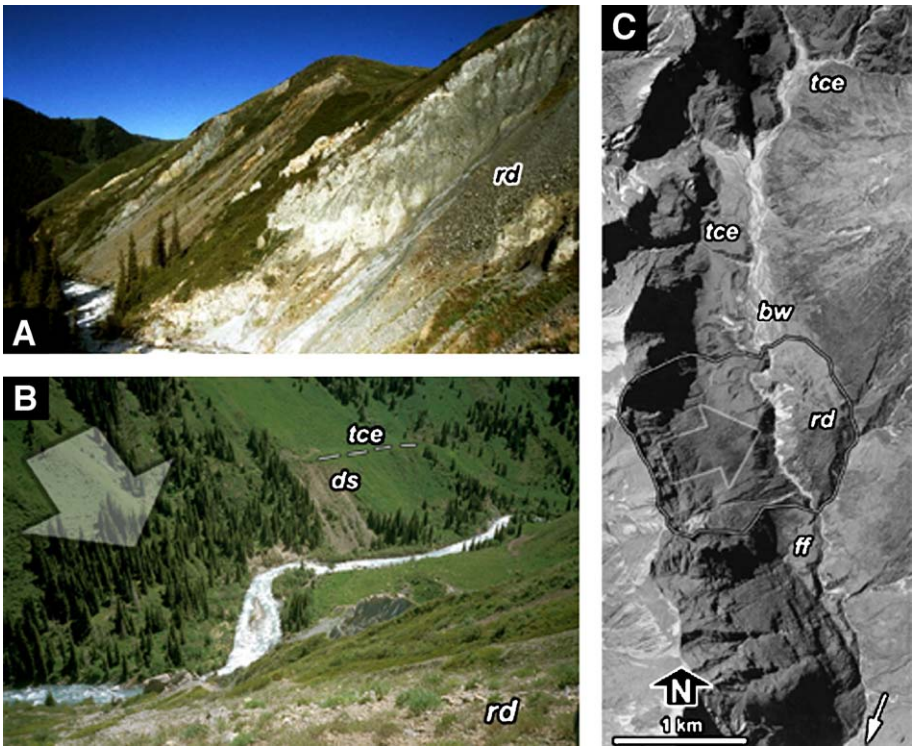

Fig. 6. Preserved breach gorges of Holocene rockslide dams. (A) Upstream view of Chon Kemin River gorge incised through shattered debris (rd) exposed in Djashilkul rockslide scar, Tien Shan. (B) View across Djashilkul re-vegetated breach gorge from top of dam (rd), with debris slide (ds) from breach terrace (tce) riser. White → indicates original rockslide movement. (C) Dissected rockslide dam (rd), Polnoon Burn, ESA, New Zealand; bw = backwater aggradation; tce = terraces indicating former lake level; ff = outburst debris. Note meander in upper breach gorge. Orthophoto courtesy of Land Information New Zealand, Crown Copyright reserved (F40 Wanaka 2002/03, www.linz.govt.nz).

of the Southern Alps (Fig. 8A). A small portion of the deposit now forms Taruahuna Pass (1252 m a.s.l.), whereas the main body of the rock avalanche travelled for 4.5 km along the headwaters of Otehake River West Branch, WSA. The valley was infilled with $\sim 55 \times 10^6$ m^3 of highly fragmented, angular greywacke and argillite debris (Korup et al., 2004). Trimlines preserved along the valley sides ~80 m above the present channel bed record the extent of the hummocky rock-avalanche debris over ~1.4 km^2 (Fig. 8B). The river has responded by cutting a steep gorge into the debris downstream of several seepage

Table 3
First-order estimates of averaged rates of geomorphic process for selected (∗ = historic) rockslide dams and lakes

Location	Infill Volume (10^6 m^3)	Infill time (years)	Eroded Volume (10^6 m^3)	Infill rate (m^3 year^{-1})	Upstream specific yield (m^3 km^{-2} year^{-1})	Downstream discharge (m^3 year^{-1})	Downstream specific yield (m^3 km^{-2} year^{-1})
Jagat/Labubesi*	50	<17	–	$>2.9 \times 10^6$	790–940	–	–
Gohna Tal*	80	78	–	1.0×10^6	4050	–	–
Tal	10	200	–	50000	21	–	–
Ghatta Khola	1	–	–	>10000	–	–	–
Dukur Pokhari	75	<1000	–	>7500	>12	–	–
ZigZag	9	–	10	>4870	>340	>5400	>370
Polnoon Burn	45	~2000	40	22500	710	19500	620
Falling Mountain*	–	–	12	–	–	1.7×10^5	18800
Latamrang	160	120	1000	1.3×10^6	760	1.9×10^5	110
Mt. Adams*	–	–	5	–	–	1.7×10^6	33300

Required (minimum) up- and downstream discharge/yield are derived from volume of infill and eroded debris, respectively; "–" = data not available.

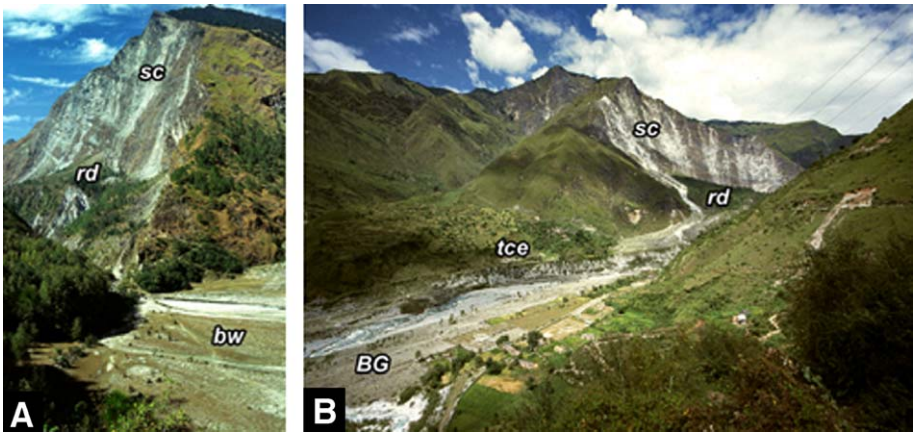

Fig. 7. 1893 Gohna Tal rockslide dam, Birahi Ganga (BG), Garhwal Himalaya, India. (A) Downstream view of headscarp (sc) and rockslide dam (rd), and backwater aggradation (bw). (B) Upstream view to blockage site. Terrace indicates deposition from catastrophic dam failure(s).

springs (Figs. 8C,D and 9). Reworked rock-avalanche debris and sediments from tributary ravines were trapped in swales on the deposit surface. An estimated 12×10^6 m^3 have been eroded since 1929 (Korup et al., 2004), and partly deposited in a dissected fan downstream from the landslide toe.

Another rock avalanche occurred in 1999, eroding $10–15\times10^6$ m^3 of schist and colluvium from the summit of Mt. Adams (2202 m a.s.l.) without any observed trigger, and formed a 100-m high dam on Poerua River, WSA. The dam lasted 6 days despite overtopping, and failed during a minor flood.

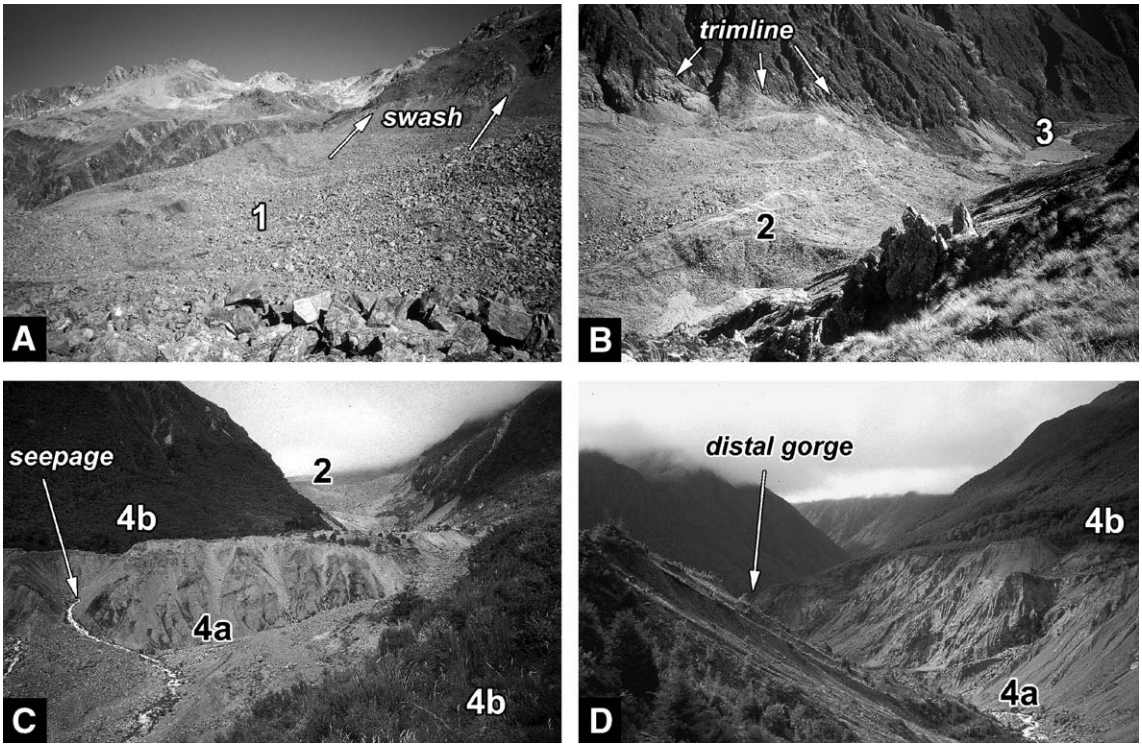

Fig. 8. 1929 Falling Mountain rock avalanche, WSA, New Zealand. (A) Deposit near Taruahuna Pass with ~60-m high swash marks. (B) Upper deposit and trimlines. (C) Dissected rock-avalanche deposit with seepage spring and re-incised gorge. (D) Down-valley view of distal deposit. Numbers refer to Fig. 9.

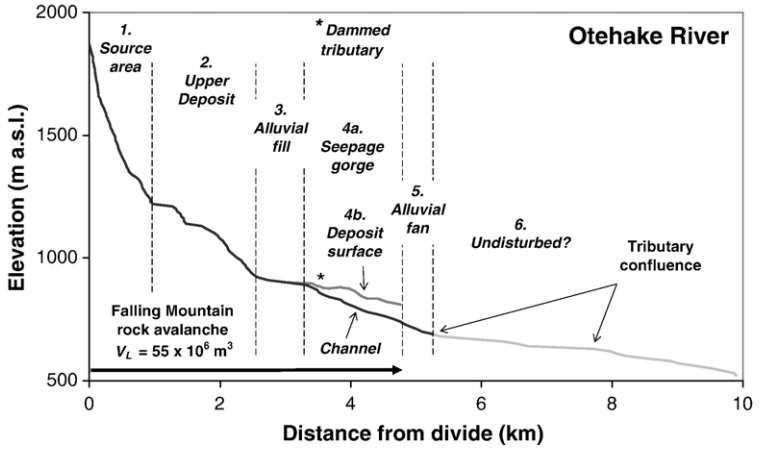

Fig. 9. Long profile of 1929 Falling Mountain rock avalanche (WSA, New Zealand), which catastrophically infilled W Branch Otehake River up to ~80 m without major blockage. The river incised a 2-km long gorge into the fragmented and easily erodible debris downstream of several seepage springs. Numbers refer to Fig. 8.

Subsequently, $\sim 5 \times 10^6$ m^3 of rock-avalanche debris and upstream sediment rapidly infilled a 3.8-km long high-energy bedrock gorge ($\Omega \sim 10^4$ W m^{-2}), forming several alluvial flats 10–20 m thick (Korup et al., 2004). The channel adjusted mainly by aggradation and more than tenfold widening of its active bed, although the steepest reaches escaped significant channel widening (Fig. 10). By 2002, ~0.07 km^2 of hillslopes were undermined, issuing shallow secondary landslides, whereas a major avulsion developed on the alluvial fanhead at the mountain front downstream.

4.5. Quantifying fluvial response from river long profiles

We used our field observations to map the position of rockslide-affected reaches along river long profiles. The results from quantitative analysis of long profiles show that the highest values of k_s are frequently located where channels were blocked by large rockslides and rock avalanches, and where rivers have re-incised into the debris (Fig. 11A–E). These dam-breach channels have high mean gradients (S=0.013–0.166; Table 2), and are characterized by peak values of k_s, which are 3–4 times higher than that of the profile average. Comparably high values for steepness are characteristic for glacially scoured bedrock steps or tributary confluences, but also for reaches along the toes of large non-blocking rock-slope failures (Fig. 11F).

Given the assumptions of downstream hydraulic geometry of $Q \propto A_C^b$, and $w \propto A_C^d$, where b and d are empirical constants, we anticipate a linear relationship between Ω [W m^{-2}] and k_s [m$^{0.9}$] in log–log space (Fig. 11G). Hence, we can use k_s as a proxy for specific stream power, which in many of the dam-breach channels also tends to be among the highest (>10^3 W m^{-2}) along the profiles studied.

Variation in k_s subsumes other controls on the shape of river long profiles, such as lithology, uplift, or sediment supply (Hodges et al., 2004). Therefore, not all knickpoints in the river long profiles are necessarily tied to large rock-slope failures. Nonetheless, most of the major knickpoints conspicuously coincide with the location of rockslide-dam breach or bypass channels (Figs. 5 and 11).

5. Discussion

5.1. Fluvial response and the life time of rockslide dams and lakes

Despite the notion that many historic landslide dams are short-lived (Ermini and Casagli, 2003), we find that long-term (10^3–10^4 year) blockage of large rivers (e.g. Kali Gandaki, Naryn) can occur. Locally, even neoglacial advances have not fully erased large rockslide deposits from the geological record (Fig. 3), although not all deposits from large rock-slope failures are preserved equally well, and some may be eroded rapidly (Fig. 10). Yet, impounded lakes can persist for up to 10^4 years before infill or dam failure.

This raises the question as to over what timescales large rockslide dams may control fluvial response.

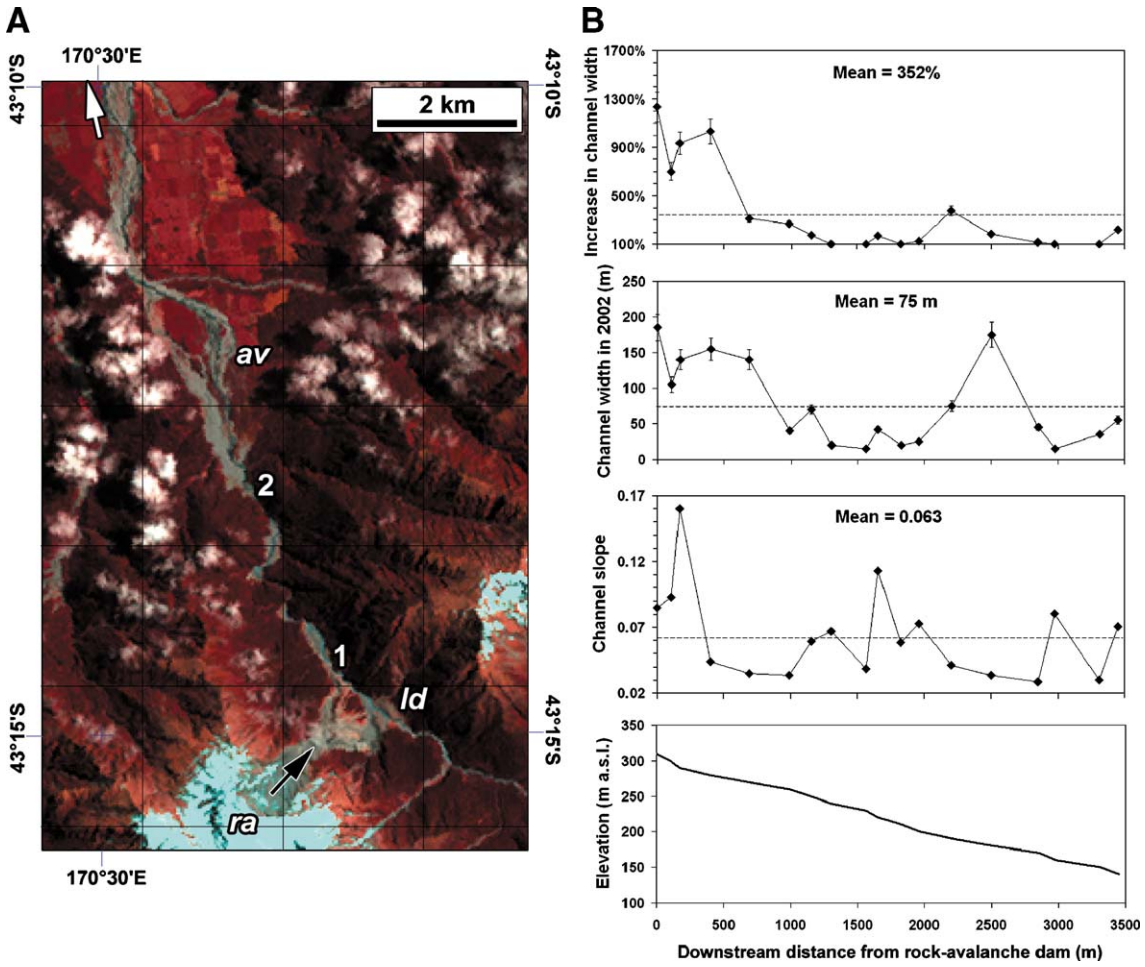

Fig. 10. (A) Landsat ETM+subscene (path 75, row 90; bands 5, 3, 2 RGB; 31 December 2002) of 1999 Mt. Adams rock avalanche, WSA, New Zealand; ra=rock avalanche (black → indicates failure movement); ld=breached landslide dam; av=landslide-induced fanhead avulsion. (B) Downstream variation of channel geometry in Poerua gorge between "1" and "2" (white → indicates flow). Elevation and gradient data refer to pre-1999 channel. Channel width w and its relative increase were measured from 1984 and 2002 air photographs at ±10% accuracy. Image courtesy of Global Land Cover Facility, University of Maryland.

Ermini and Casagli (2003) presented a geomorphometric method for empirically classifying stable and unstable landslide dams using a dimensionless blockage index (DBI) based on dam volume, height, and upstream catchment area. We find that eight of the breached rockslide dams we studied plot within the stable domain (Fig. 12).

The rockslide dams of Latamrang and Polnoon Burn, for example, had impounded lakes for 10^2 and 10^3 years, respectively, and these dams could well have been classified as "stable" during these periods. Yet despite these dam breaches the adjustment in the river long profile appears to be incomplete (Fig. 5). Obviously, distinguishing between the life span of a dam and the lake it impounds is important. Even if a dam should remain intact over the time needed to infill the reservoir, catastrophic overtopping and lake discharge may occur via an epigenetic bypass gorge (Fig. 2).

Long-lived rockslide-dammed lakes may result from the favourable combination of several factors such as very large dam size ($>10^9$ m^3) and (semi-) arid climate in headwaters, with Q being lower for a given A_C than in more humid basins (Fig. 12). None of the numerous large prehistoric rockslides known in the perhumid WSA have retained lakes to the present, and scaling relationships between the size of the landslide and upstream catchment area were inadequate for predicting the type of observed fluvial response (Korup, 2004b, 2005). There, and also in the Indian and Nepal Himalayas, most historic rockslide dams are not as large and commonly

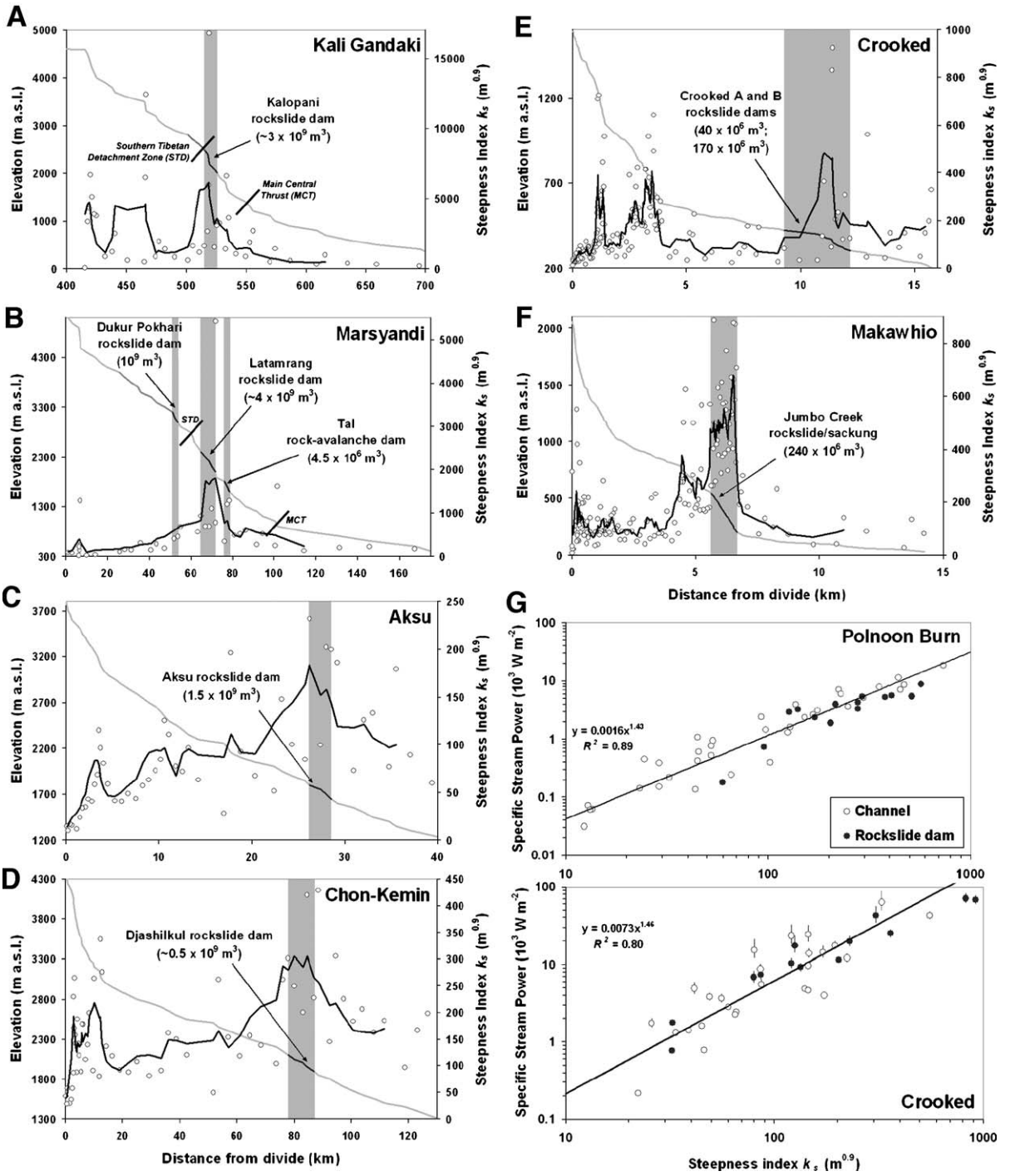

Fig. 11. (A–F) River long profiles (grey lines) with variation of steepness index k_s (white dots) and its 5-point running mean (black lines) for fixed concavity index $\theta = 0.45$ show spatial coincidence between high values of k_s and deposits from large rockslides (grey-shaded boxes). (G) Empirical relationship between specific stream power and k_s, derived from Eq. (2) for two rivers impacted by rockslide dams. See text for explanation.

short-lived (e.g. Gohna Tal, Jagat, and Labubesi). High (monsoonal) precipitation, sediment yields, and upstream relief (Table 2) are reasons other than geotechnical susceptibility to failure that may explain the short life spans and the general scarcity of rockslide-dammed lakes in these regions.

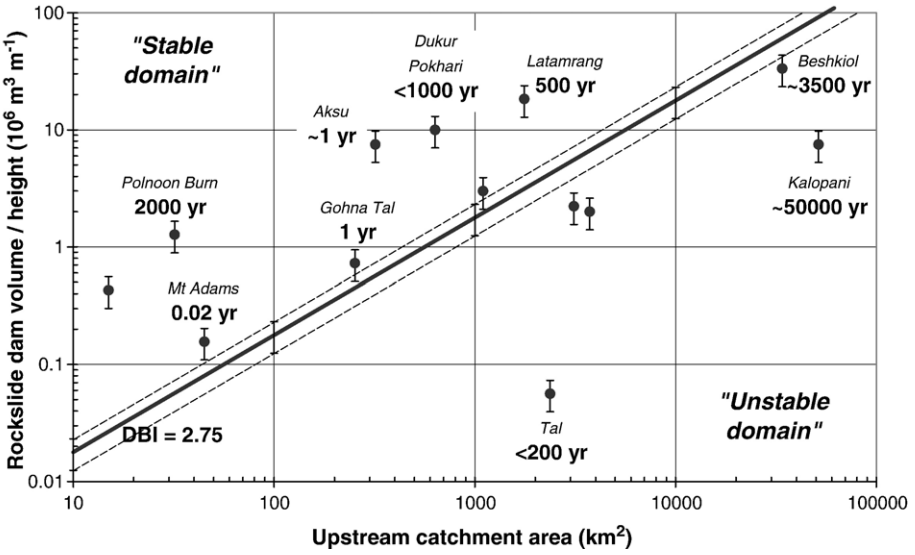

Fig. 12. The volumes of rockslide dams scaled by height versus upstream catchment area for case studies (bars indicate ±30% error). Diagonal line is "critical" Dimensionless Blockage Index (Ermini and Casagli, 2003) DBI=2.75 for world-wide data, separating empirically derived "stable" from "unstable" domains of landslide dams. Both ephemeral rockslide-dammed lakes and some that persisted for 10^3–10^4 years plot in the "stable domain".

5.2. Fluvial response recorded in sediment budgets

Most large rockslide dams studied produced significant volumetric changes to catchment sediment budgets. Although breached, many of the rockslide/avalanche dams we studied have retained more than half of the original volumes (Table 3). Backwater aggradation formed wedges of alluvial bed-load, lacustrine, and hillslope deposits, of several kilometres in length. We estimate, for example, that $\sim 10^{10}$ m^3 were deposited upstream of the Beshkiol rockslide. Comparable figures were reported from fills behind large rock-avalanche dams in the Karakoram (Hewitt, 1998). We note that these are order-of-magnitude estimates because of unknown trapping efficiency.

Historic examples demonstrate that, shortly after breaching, large amounts of debris can be eroded from rockslide and rock-avalanche dams, producing discharge and yield rates of up to 10^6 m^3 year^{-1} and 10^4 m^3 km^{-2} year^{-1}, respectively (Table 3). The Falling Mountain rock avalanche (Fig. 8) shows that high yields also occur without major blockage. These figures surpass long-term catchment rates and highlight the importance of rockslide-derived sediment pulses in high mountain rivers and the role of sediment yield as an important fluvial response variable (Fig. 10).

However, we caution against the linear extrapolation of sediment delivery from prehistoric rockslide dams through time, because it is possible that most of their erosion took place in the years following initial breaching (Table 3). Because we do not know how frequently large river-damming rock-slope failures occur in the study areas, it is presently not feasible to assess their importance to long-term sediment budgets.

5.3. Fluvial response recorded in the river long profile

In many tectonically active mountain belts steady-state conditions, i.e. statistical balance between uplift and erosion, have been invoked on 10^6-year timescales, in which fluvial incision of bedrock in response to regional uplift would set the pace for rather passive adjustment of hillslopes (see Whipple, 2004 for a detailed review).

On 10^3–10^4-year timescales, i.e. the residence times of the Kalopani, Polnoon Burn, Zig-Zag, Beshkiol, and possibly, many other rockslides, however, disequilibrium conditions may prevail (Pratt-Sitaula et al., 2004), especially if rockslide dams occur along a river repeatedly and more frequently than it would take for the river to recover from the impact. Hewitt (1998) highlighted this distinctive control of large ($>10^6$ m^3) catastrophic rockslides on the fluvial geomorphology of the upper Indus River, Pakistan. The examples of the Kali Gandaki, Marsyandi, and Chon-Kemin Rivers show that such river "segmentation" by large rockslides also occurs elsewhere.

The most pronounced disequilibrium effects are blockage and backwater aggradation, which in our examples affect between 1–37% and 2–20% of total channel length and basin relief, respectively (Table 2). Aggradation behind the Kalopani rockslide, for example, has inhibited river erosion into bedrock along the Tibetan reach of the Kali Gandaki since at least 50–60 ky (Lavé and Avouac, 2001). This effect of dampening fluvial response to tectonic uplift is pronounced in semi-arid Ladakh, NW Indian Himalaya, where several deposits of long-lived Pleistocene rockslide-dammed lakes remain (Fort et al., 1989; Phartiyal et al., 2005).

Contact avulsions caused by rockslides (Korup, 2004b) may shift the focus of fluvial erosion. The Naryn River, for example, was forced to erode ~1.3 km^3 of bedrock around the toe of the Beshkiol rockslide (Fig. 2), thus, repeating bedrock incision along this 10-km long epigenetic gorge.

Dam-breach channels with some of the highest values of steepness index k_s and inferred specific stream power Ω along a given profile have developed below conspicuous knickpoints (Figs. 5C, D and 11A–E). This confirms our hypothesis that channel gradient would record long-term fluvial response to large rock-slope failures. We do not find any robust correlation, however, between peak values of k_s and rockslide size, with rockslide dam height H_D, for instance, explaining <50% of the variation in k_s. The preservation of large (>10^6 m^3) Mid-Holocene rockslide deposits on active valley floors, however, is seemingly at odds with high specific stream power (Fig. 11) and high rates of long-term fluvial incision into valley fill and bedrock (Fig. 5).

We speculate that high rates of fluvial incision promote the preservation of rockslide debris, once dissected or bypassed by steep gorges (Fig. 5A). Controlled by local gradient and high uplift, many of these high-energy reaches do not appear to have the potential for effective lateral erosion other than triggering secondary debris slides until breach channel flanks have stabilized. Furthermore, large rockslide boulders add to boundary resistance and surface armouring in steep channels. Locally, W/D in these channel reaches may be as low as ~0.2, especially where they formed epigenetic slot gorges in response to blockage (B. Pratt-Sitaula, personal communication, 2005).

Naturally, some of the knickpoints may also be tied to structural or lithological boundaries, such as the Kalopani rockslide dam, which is located near the Southern Tibetan Detachment Zone (Fig. 11A). Locally, it is also possible that bedrock channel knickpoints or significantly steep reaches could have predated or even contributed to rock-slope failure by fluvial undercutting, especially where steep channel reaches coincide with large non-blocking rock-slope failures (Fig. 11F). Yet, the majority of the channel reaches in question are cut into rockslide debris (Figs. 1, 3 and 6)), so that knickpoints are highly likely a result of rock-slope failure rather than the other way around. This illustrates that mountain rivers also need to respond and adjust to large-scale disturbances from hillslope processes on 10^1–10^4 year timescales, rather than being invariably capable of setting the pace for hillslope adjustment (Whipple and Tucker, 1999).

6. Conclusions

Deposits of large (10^7–10^{10} m^3) Late Pleistocene to Holocene river-blocking rock-slope failures are preserved in the Himalayas, the Tien Shan, and the Southern Alps in New Zealand despite high rates of uplift and fluvial erosion. These deposits control fluvial response by

(a) retaining sediment and forcing alluviation of 10^6–10^{10} m^3;
(b) relocating river channels through diversion or seepage;
(c) delaying fluvial bedrock incision by promoting aggradation behind rockslide dams;
(d) forming steep high-energy breach channels with knickpoints and knickslopes in channel long profiles; and
(e) shaping valley-floor morphology on 10^1–10^4 year timescales. Sediments indicate that rockslide-dammed lakes may persist over 10^0–10^4 years, before being drained or infilled. Although smaller (10^7–10^8 m^3) and comparably short-lived (10^0–10^2 year), several historical rockslide dams induced short-lived pulses to catchment sediment budgets within a few years or decades following failure, which should not be linearly extrapolated through time for prehistoric events. Existing rockslide-dammed lakes are rare in all study areas, not necessarily solely because of geotechnical susceptibility to failure, but also because of high discharge causing rapid infilling or overtopping.

Future research will examine what degree of fluvial recovery from rockslide dams may be measured and modelled in terms of changes to the long profile, or

equilibrium conditions of reach-scale sediment in- and output. More absolute age constraints will be needed to better assess the magnitude, frequency, and life span of large rock-slope failures that block rivers.

Acknowledgements

This paper is a contribution to IPL-M117 "Geomorphic hazards from landslide dams" of the International Consortium on Landslides (ICL). We thank Beth Pratt-Sitaula and Michelle Garde for allowing us to use unpublished data on the Marsyandi River. Anatoliy Zhirkevitch gave useful comments on hydrology in the Tien Shan. We greatly appreciate the critical reviews of Ellen Wohl, Timothy R.H. Davies, and Daniel Miller.

References

Abdrakhmatov, K., Aldazhanov, S.A., Hager, B.N., et al., 1996. Relatively recent construction of the Tien Shan inferred from GPS measurements of present-day crustal deformation rates. Nature 384, 450–457.

Chai, H.J., Liu, H.C., Zhang, Z.Y., Xu, Z.W., 2000. The distribution, causes and effects of damming landslides in China. Journal of Chengdu University of Technology 27, 302–307.

Chedia, O.K., 1986. Morphostructures and Neotectonics of the Tien Shan. Ilim Publishers, Frunze. 315 pp. (in Russian).

Clague, J.J., Evans, S.G., 1994. Formation and failure of natural dams in the Canadian Cordillera. Geological Survey of Canada Bulletin 464 (35 pp.).

Costa, J.E., Schuster, R.L., 1988. The formation and failure of natural dams. Geological Society of America Bulletin 100, 1054–1068.

Cruden, D.M., Varnes, D.J., 1996. Landslide types and processes. In: Turner, A.K., Schuster, R.L. (Eds.), Landslides, investigation and mitigation. Special Report, vol. 247. Transportation Research Board, National Research Council, pp. 36–75.

Delvaux, D., Abdrakhmatov, K.E., Lemzin, I.N., Strom, A.L., 2001. Landslides and surface breaks of the 1911, M_s 8.2 Kemin earthquake, Kyrgyzstan. Russian Geology and Geophysics 42, 1583–1592.

Ermini, L., Casagli, N., 2003. Prediction of the behaviour of landslide dams using a geomorphological dimensionless index. Earth Surface Processes and Landforms 28, 31–47.

Fort, M., 2000. Glaciers and mass wasting processes: their influence on the shaping of the Kali Gandaki Valley (higher Himalaya of Nepal). Quaternary International 65/66, 101–119.

Fort, M., Burbank, D.W., Freytet, P., 1989. Lacustrine sedimentation in a semiarid alpine setting: an example from Ladakh, northwestern Himalaya. Quaternary Research 31, 332–350.

Henderson, R.D., Thompson, S.M., 1999. Extreme rainfalls in the Southern Alps of New Zealand. Journal of Hydrology (New Zealand) 38, 309–330.

Hewitt, K., 1998. Catastrophic landslides and their effects on the Upper Indus streams, Karakoram Himalaya, northern Pakistan. Geomorphology 26, 47–80.

Hewitt, K., 2002. Postglacial landform and sediment associations in a landslide-fragmented river system: the Transhimalayan Indus streams, Central Asia. In: Hewitt, K., Byrne, M.L., English, M., Young, G. (Eds.), Landscapes of transition. Landform assemblages and transformations in cold regions. Dordrecht, Kluwer, pp. 63–91.

Hodges, K.V., Wobus, C., Ruhl, K., Schildgen, T., Whipple, K.X., 2004. Quaternary deformation, river steepening, and heavy precipitation at the front of the Higher Himalaya ranges. Earth and Planetary Science Letters 220, 379–389.

Hormann, K., 1974. Die Terrassen des Seti Khola-Ein Beitrag zur Quartären Morphogenese in Zentral Nepal. Erdkunde 28, 161–176.

Ignatiev, I.V., 1886. Earthquake in the Tokmak District in 1885. Proceedings of the Imperial Russian Geographic Society 22, 150–164. (in Russian).

Jacobsen, J.P., 1990. Die Vergletscherungsgeschichte des Manaslu Himalayas und ihre klimatische Ausdeutung. Geo Aktuell, vol. 1. Terrimago-Pachnicke, Göttingen. 76 pp.

Knighton, A.D., 1998. Fluvial forms and processes. Arnold, London. 383 pp.

Korup, O., 2004a. Geomorphometric characteristics of New Zealand landslide dams. Engineering Geology 73, 13–35.

Korup, O., 2004b. Landslide-induced river channel avulsions in mountain catchments of southwest New Zealand. Geomorphology 63, 57–80.

Korup, O., 2005. Distribution of landslides in southwest New Zealand. Landslides 2, 43–51.

Korup, O., McSaveney, M.J., Davies, T.R.H., 2004. Sediment generation and delivery from large historic landslides in the Southern Alps, New Zealand. Geomorphology 61, 189–207.

Lavé, J., Avouac, J.P., 2001. Fluvial incision and tectonic uplift across the Himalayas of central Nepal. Journal of Geophysical Research 106 (B11), 26561–26591.

Long, D.T., Cox, S.C., Bannister, S., Gerstenberger, M.C., Okaya, D., 2003. Upper crustal structure beneath the eastern Southern Alps and the Mackenzie Basin, New Zealand, derived from seismic reflection data. New Zealand Journal of Geology and Geophysics 46, 21–39.

Makarov, V.I., 1977. Newest tectonic structure of the Central Tien Shan. Science Publishers, Moscow. 172 pp. (in Russian).

McSaveney, M.J., 2002. Recent rockfalls and rock avalanches in Mount Cook National Park, New Zealand. In: Evans, S.G., DeGraff, J.V. (Eds.), Catastrophic landslides: effects, occurrence, and mechanisms, vol. XV. Geological Society of America Reviews in Engineering Geology, pp. 35–70.

Molnar, P., Tapponier, P., 1975. Cenozoic tectonics of Asia. Effects of a continental collision. Science 189, 419–426.

Norris, R.J., Cooper, A.F., 2000. Late Quaternary slip rates and slip partitioning on the Alpine Fault, New Zealand. Journal of Structural Geology 23, 507–520.

Phartiyal, B., Sharma, A., Upadhyay, R., Sinha, A.K., 2005. Quaternary geology, tectonics and distribution of palaeo-and present fluvio/glacio lacustrine deposits in Ladakh, NW Indian Himalaya—a study based on field observations. Geomorphology 65, 241–265.

Pratt-Sitaula, B., Burbank, D.W., Heimsath, A., Ojha, T., 2004. Landscape disequilibrium on 1000–10,000 year scales, Marsyandi River, Nepal, central Himalaya. Geomorphology 58, 223–241.

Pushkarenko, V.P., Nikitin, A.M., 1988. Experience in the regional investigation of the state of mountain lake dams in central Asia and the character of breach mudflow formation. In: Kozlovskii, E.A. (Ed.), Landslides and Mudflows. UNEP/UNESCO, Moscow, pp. 359–362. (in Russian).

Saijo, K., Tanaka, S., 2002. Paleosols of middle Holocene age in the Thakkola basin, central Nepal, and their paleoclimatic significance. Journal of Asian Earth Sciences 21, 323–329.

Schramm, J.-M., Weidinger, J.T., Ibetsberger, H.J., 1998. Petrologic and structural control on geomorphology of prehistoric Tsergo Ri slope failure, Langtang Himal, Nepal. Geomorphology 26, 107–121.

Strom, A.L., 1998. Giant ancient rock slides and rock avalanches in the Tien Shan Mountains, Kyrgyzstan. Landslide News 11, 20–23.

Strom, A.L., Abdrakhmatov, K.E., 2004. Clustering of large rockslides: the phenomenon and its possible causes. In: Lacerda, W.A., Ehrlich, M., Fontoura, A.B., Sayao, A. (Eds.), Landslides: Evaluation and Stabilization. Taylor and Francis Group, London, pp. 317–320.

Tippett, J.M., Kamp, P.J.J., 1995. Quantitative relationships between uplift and relief parameters for the Southern Alps, New Zealand, as determined by fission track analysis. Earth Surface Processes and Landforms 20, 153–175.

Upreti, B.N., 1999. An overview of the stratigraphy and tectonics of the Nepal Himalaya. Journal of Asian Earth Sciences 17, 577–606.

Weidinger, J.T., 1998. Case history and hazard analysis of two lake-damming landslides in the Himalayas. Journal of Asian Earth Sciences 16, 323–331.

Weidinger, J.T., Ibetsberger, H.J., 2000. Landslide dams of Tal, Latamrang, Ghatta Khola, Ringmo and Dharbang in the Nepal Himalayas and related hazards. Journal of the Nepal Geological Society 22, 371–380.

Weidinger, J.T., Schramm, J.-M., Nuschej, F., 2002. Ore mineralization causing slope failure in a high-altitude mountain crest—on the collapse of an 8000-m Peak in Nepal. Journal of Asian Earth Sciences 21, 295–306.

Weidinger J.T., in press. Landslide dams in the high mountains of India, Nepal and China — stability and life span of their dammed lakes. Proceedings NATO Advanced Research Workshop on the Security of Natural and Artificial Rockslide Dams, Bishkek, Kyrgyzstan, 8–13 June 2004, Springer.

Whipple, K.X., 2004. Bedrock rivers and the geomorphology of active orogens. Annual Reviews in Earth and Planetary Sciences 32, 151–185.

Whipple, K.X., Tucker, G.E., 1999. Dynamics of the stream-power river incision model: implications for height limits of mountain ranges, landscape response times, and research needs. Journal of Geophysical Research 104 (B8), 17661–17676.

Whitehouse, I.E., 1988. Geomorphology of the central Southern Alps, New Zealand: the interaction of plate collision and atmospheric circulation. Zeitschrift für Geomorphologie NF 69, 105–116.